This article has been accepted for publication in IEEE Journal of Emerging and Selected Topics in Power Electronics. This is the author's version which has not been fully edited and content may change prior to final publication. Citation information: DOI 10.1109/JESTPE.2024.3486554

Sector Wise Modified Droop Control to Improve Voltage Regulation and Current Sharing in Parallel Boost Converter Interfaced DC Microgrid

Makireddi Ramana[1], Subhendu Bikash Santra[2*] *Senior Member IEEE*, Debashis Chatterjee[4], Yam P. Siwakoti[3] *Senior Member IEEE*

[1]School of Electronics Engineering KIIT DU., [2]Department of Electrical Engineering, Shiv Nadar Institution of Eminence-DU, Delhi-NCR, [3]School of Electrical and Data Engineering, University of Technology Sydney, Australia, [4]Department of Electrical Engineering Jadavpur University-WB, India. * *Corresponding author Email ID*: Subhendu.santra@snu.edu.in

***Abstract*—Photovoltaic panel (PV) interfaced multiple parallel boost converter with storage interface is essential for forming DC microgrid. Impedance shaping or droop coefficient adjustment of individual converter is essential to achieve better voltage regulation and proportional current sharing. However, the voltage droop with increased loading is not linear even with dual loop control, where outer loop is voltage mode with droop coefficient adjustment and inner one is current loop. The loading range is narrow to maintain voltage regulation within limit. This nonlinearity in droop coefficient after certain enhanced loading is due to load dependent converter output impedance and converter non idealities. In this work, a sector wise modified droop coefficient adjustment control is proposed which ensures enhanced loading operation of individual converter while maintaining the voltage regulation constraints. This article also proposes an optimal droop coefficient, enhancing current distribution, which ultimately decreases circulating current and conduction losses. The proposed control method is simulated in PSIM and experimentally validated in 1.5kW, 48V ELVDC Microgrid Set-Up.**

***Index Terms*—Droop control, Parallel Boost DC-DC Converter, Voltage Regulation and Current sharing.**

I. Introduction

Multiple parallel connected converter-based DC microgrid structure is common in small and medium power (2 kW-5 kW) residential system [1]. Generally, boost converter is necessary to interface the inherent low voltage from PV panel with maximum power point tracking (MPPT) to generate stable high voltage for DC link and to extract maximum power under different environmental conditions. The common DC link voltage is generally categorised as Low Voltage DC (LVDC) for 380V-400V and Extra Low Voltage (ELVDC) for 24V-48V. The DC link voltage using multiple PV integrated converter is susceptible to parametric variation of individual converter, irradiation (G) variation, operating point shifting etc. Therefore, maintaining the DC link voltage with proportional current sharing is challenging in such LVDC or ELVDC systems [2], [3]. Additionally, a circulating current within converter is major problem in such system which increase the conduction loss and thereby reduce the system efficiency.

Several solutions exist based on droop coefficient adjustment of individual converter operated in parallel. The operation is like DC generators connected in parallel. However, the control is not similar, as ELVDC is power electronics converter dominated system with uncertainties in PV power generation which is the primary energy source. The output impedance of a boost converter [4] is constant for a duty ratio with constant switching frequency and source voltage. This output impedance can be varied by changing the duty ratio which is termed as droop coefficient adjustment, and it helps to regulate common DC link voltage and current sharing in multiple parallel connected converter system in DC microgrid [5]. However, the droop coefficient is not constant throughout loading range of each converter. It has both constant and load dependent part which creates non-linearity in droop characteristics (V-I) of boost converter. To validate, two separate boost converters with different ratings i.e. 250 W shown in Fig. 1 (a) and 1.5 kW shown in Fig. 1 (c) are tested. The droop characteristics for these converters for duty ratio 0.5 and 0.4, are shown in Fig. 1 (b) and Fig. 1 (d) respectively.

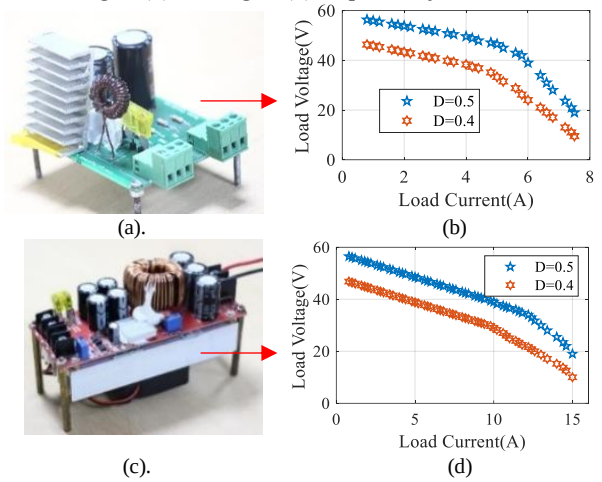

Fig. 1. Nonlinear droop coefficient for practical boost converter: (a) 250 W boost converter (b) droop characteristics for 250 W (c) 1.5 kW boost converter (d) droop characteristics for 1.5 kW.

This nonlinearity in the droop characteristics creates large variation in common DC link voltage beyond certain loading. Thus, maintaining DC link voltage regulation (VR) and proportional current sharing within limit is difficult. This nonlinearity in droop coefficient with the source variation (PV power generation) and parametric variation further limits the loadability of ELVDC grid, even with dual loop control either using (a) outer current loop with droop coefficient adjustment and inside voltage mode loop or (b) outer voltage loop with droop coefficient adjustment and inner current loop [6]. Other approaches like DC signaling method and Master Slave control [7] are also implemented to solve this issue. However, these solutions are communication dependent and prone to single point failure [8]. Solution by M. Ashourloo *et.al*. [8] needs minimum burden on communication is promising.

Droop control is simple and has minimum communication requirements with easy implementation in primary control of hierarchical framework [9]. The droop control method in DC microgrid which is extensively used for primary control can be broadly divided into four major categories i.e. (a) Conventional droop control, (b) Non-linear droop control, (c) Piecewise droop control (d) Other hybrid methods as shown in Fig. 2.

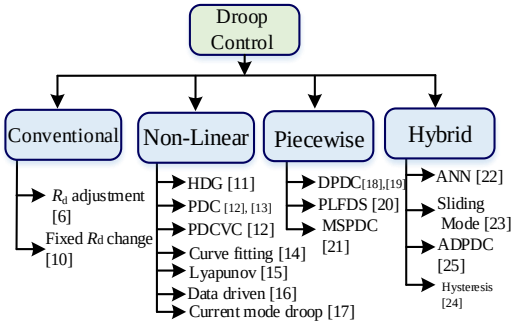

Fig. 2. Different droop control methods for DC microgrid.

This article has been accepted for publication in IEEE Journal of Emerging and Selected Topics in Power Electronics. This is the author's version which has not been fully edited and content may change prior to final publication. Citation information: DOI 10.1109/JESTPE.2024.3486554

Conventional droop control [6] has poor VR and higher current sharing difference (CSD). To overcome large VR and CSD, a fixed set of droop coefficient (R_d) change is proposed [10] which is limited by the selection of droop gains (K_1, K_2) and storing in look up table. Non-linear droop control method is an alternative to conventional where precious value of droop coefficient can be calculated which improves both VR and CSD. High droop gain (HDG) method [11] is a non-linear droop control method which has poor CSD at intersection point of linear and non-linear section of droop curve. Polynomial droop curve (PDC) method [12] accurately emulates non-linear droop curve. However, this method has poor VR at rated loading condition. This problem can be reduced by adding voltage compensation in polynomial droop curve with voltage compensation (PDCVC) method [13]. But it has poor CSD performance near light loading due to asymmetry. Other recent approaches in non-linear droop control are curve fitting method [14], Lyapunov method [15], data driven non-linear droop [16] and current mode droop [17]. These methods provide good VR and CSD but with major limitations like increased complexity, light load performance, parameter dependency and data accuracy.

These complexities of the non-linear droop control method can be resolved by using simplified piecewise droop control where the droop characteristics are segmented into number of linear sections. Multi-section piecewise droop control (MSPDC) [18] having good VR and CSD performance but excessive sections to fit droop curve provides slow response under dynamic conditions and poor CSD performance at light loading. Thus, lower number of section-based droop control (piecewise linear formation of droop strategy (PLFDS)) is tried for achieving good performance [19]. However, tuning of different sections depends on loading and calculation is complex which restricts online application. To overcome this difficulty, distributed piecewise droop control (DPDC) is proposed by S.Liu *et.al.* [20]-[21] which is a promising solution. The main difficulty in realizing adaptive switches between different sections of droop curve and calculation of offset voltage coefficient (K_n) parameter.

Combining the advantages of non-linear and piecewise droop control, hybrid methods have emerged like ANN based [22], sliding mode adaptive droop control [23], hysteresis based [24] and adaptive discrete piecewise droop control (ADPDC) [25]. The ANN method is limited by training accuracy as it is done offline and may not converge on real application. Similarly, in [23] there is a problem of defining fuzzy optimizer function which mainly depends on membership function and difficult to obtain considering converter parameters, cable resistance and PV power variation. ADPDC is the promising advancement over DPDC method. This work mainly focuses on continuously updating the reference voltage from the current error [reference to actual converter output current] which makes it possible to track the exact droop coefficient value. The meaning continuously here is updating the reference voltage value after certain time value which is guided by the transient time of DGs under load change. Thus, the accuracy of the droop coefficient tracking is good and provides better results during steady state and in transient. However, the limitation is designing integrator gain (K_i) value is complex and has significant computation burden. Another problem is setting the accurate reference current especially at starting time. For improper selection of K_i the controller will not converge and circulating current can further enhance the reference current. This makes instability in settling two separate DG voltages.

As per literature, the research gaps are still existing like simplifying droop characteristics emulation without increasing control complexity and see the effects of PV panel characteristics with cable resistance, duty ratio range etc. The submitted work is mostly on the simplification of control structure using a mixed model [linear and piecewise section (three sections)]. It firstly removes the complexity of continuously finding droop coefficient to a range of 50% of maximum loading capacity of the connected converter by finding optimal droop coefficient which takes care of minimum conduction loss and CSD. This also solves the problems associated with light and medium loading (problems present in discrete piecewise droop control). For enhanced loadability (beyond 50% loading) without much compromising on VR and CSD three piecewise sections are considered for the implementation. Also, in this work PV characteristics impact on finding the operating duty ratio is proposed which is more on practical side. This study helps to make primary control simplified and thus plug and play feature can be implemented easily in the secondary control.

II. Voltage Regulation And Current Sharing Behaviour of Parallel PV-Boost Converter System

A. *Open Loop Control Without MPPT:*

The general diagram of multiple parallel PV-boost converter based ELVDC Microgrid is shown in Fig. 3. As the power generation from PV panel is highly dependent on environmental conditions, so storage is an essential part which manages the power mismatch from generation to load demand. Additionally, conventional AC power can also be used after rectification for managing load requirement.

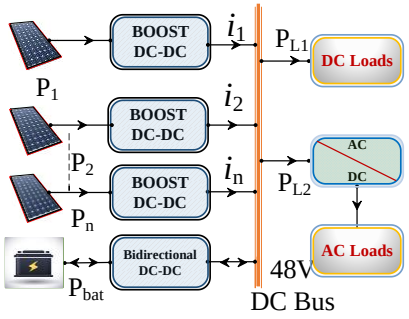

Fig. 3. Multiple PV string fed boost converters connected with ELVDC bus.

In this section, for analysing the individual converter output, common DC link voltage and current sharing, simple power flow condition is considered, i.e., generated power is greater than load power requirement as in (1).

$$P_{L1} + P_{L2} \leq \sum_{i=1}^{n} P_i \quad (1)$$

Where, P_{L1} is the dc load demand, P_{L2} is the ac load demand and P_i is the power generation from i^{th} PV Panel. The main requirements of any parallel connected system are to maintain constant output voltage ($\Delta v_0 = v_{0max} - v_{0min} \approx 0$) and equal load sharing ($\Delta I = |I_1 - I_2| \approx |I_3 - I_4| \approx \cdots \approx |I_{n-1} - I_n| \approx 0$). Two parallel connected PV systems without storage and the steady state electrical equivalent circuit are shown in Fig. 4 (a) and Fig. 4 (b) respectively. The maximum power delivering capability of PV_1 is P_1 and for PV_2 is P_2. V_1 and V_2 are the open circuit voltages of PV_1 and PV_2 respectively. Similarly, the operating currents from both the PV panels are I_1 and I_2. The operating current range from both the PV panels are $I_{1\_min} \leq I_1 \leq I_{1\_max}$ and $I_{2\_min} \leq I_2 \leq I_{2\_max}$.

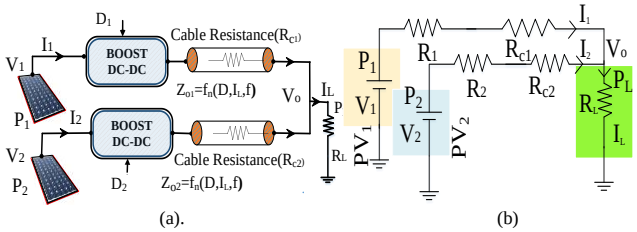

Fig. 4. (a) Two parallel PV-boost converter systems with cable resistance. (b) Steady state circuit diagram of the system.

Boost converters are operated in open loop mode where D_1 and D_2 are the open loop duty ratio. The converter output impedance is a function of duty, frequency and load current which will be added

with cable resistance R_{c1} and R_{c2} to decide the droop coefficient. It controls common DC link voltage which varies within a range of $v_{o\_min} \le v_o \le v_{o\_max}$. Individual converter voltage and current variations in ELVDC are shown in Fig. 5.

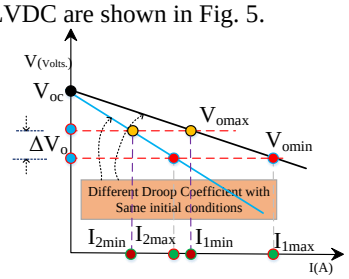

Fig. 5. Change in DC link voltage (ΔV_o) with non-uniform current sharing with different droop coefficient [10].

Due to different droop coefficients, converter load sharing varies for a constant voltage. This creates converter burden imbalance and small deviation in converter voltage creates circulating current. To achieve proportional current sharing with multiple parallel connected converters, the current ratio from individual power string should be ideally constant for all loading conditions. Applying KVL in Fig 4 (b),

$$V_o = V_1 - I_1(R_1 + R_{c1}) = V_2 - I_2(R_2 + R_{c2}) = (I_1 + I_2)R_L \quad (2)$$

$$I_1 = \frac{V_1 - V_0}{R_1 + R_{c1}}; I_2 = \frac{V_2 - V_0}{R_2 + R_{c2}} \quad (3)$$

$$\frac{I_1}{I_2} = \frac{\frac{P_1}{V_1}}{\frac{P_2}{V_2}} = \mu_p \frac{(I_1+I_2)R_L + I_2(R_2+R_{c2})}{(I_1+I_2)R_L + I_1(R_1+R_{c1})}. \quad (4)$$

Where, $\mu_P = \frac{P_1}{P_2}$

From the equation (4), current sharing ratio as function of input power, equivalent resistance and cable resistance can be derived and mentioned in equation (5). The derivation is mentioned in Appendix-I. When PV strings generate the same power, the current sharing ratio is mainly dependent on equivalent converter resistance and cable resistance. From equation (4) the variations in current sharing ratio for different PV panel power can be derived and shown in Fig. 6 (a). Similarly, converter output voltage variation (for a constant duty ratio) depends on four different conditions (Details is in Appendix-I) as mentioned in equation (6). The deviation of voltage with variable PV power is shown in Fig. 6 (b).

$$\frac{I_1}{I_2} = -x \pm y \quad (5)$$

Where,

$$x = \frac{-(1-\mu_p)}{2(1+\frac{R_1+R_{c1}}{R_L})}, y = \sqrt{\mu_p \frac{(R_2+R_{c2}+R_L)}{(R_1+R_{c1}+R_L)} + \left[\frac{(1-\mu_p)}{2(1+\frac{R_1+R_{c1}}{R_L})}\right]^2}$$

For the multiple parallel connected converters without any control have the problem of poor VR and unequal CSD.

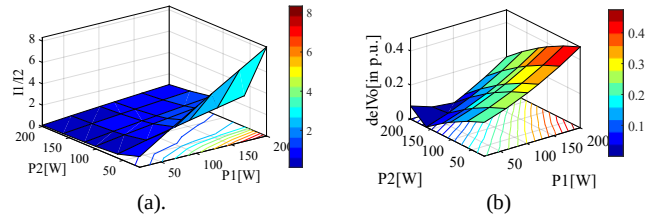

(a). (b)

Fig. 6. For variable PV power at non-MPPT mode (a) Current sharing ratio, (b) Output Voltage deviation.

B. Open Loop Control With MPPT

Power generation from each PV string varies based on temperature and irradiance. For better utilization, MPPT algorithm should be implemented to extract the maximum power from each PV string.

In this section, the impact of MPPT control on parallel PV connected converter system is discussed. For this analysis, KC 200 GT PV panel is used. The power and current equation of KC 200GT panel under different irradiance conditions are derived using curve fitting. This helps to find an empirical relationship between PV power, voltage and current. PV voltage remains almost constant at MPP, and boost converter duty ratio is changed as per MPPT algorithm to extract maximum power from each PV string. V_{MPP} and P_{MPP} relation for KC 200GT panel is derived [26] based on linear interpolation which is mentioned in equation (7). I_{MPP} and P_{MPP} relations are derived based on linear interpolation as mentioned in equation (8)

$$V_{MPP} = 9\times10^{-5}P_{MPP}^2 + 0.021\times P_{MPP} + 25.138 \quad (7)$$

$$I_{MPP} = 0.0378\times P_{MPP} + 0.0014 \quad (8)$$

The CSD and Output voltage deviation under MPPT condition for the system are mentioned in equation (9) and equation (10) [Details is in Appendix-I].

$$\Delta I = (1\text{-}D_1)CF_1I_1 - (1\text{-}D_2)CF_2I_2 \quad (9)$$

Where, $CF_i = 1 + \frac{v_d}{v_{sd}} + \frac{D_i r_{ds} + [1-D_i]r_d + r_l}{[1-D_i]^2 R_L}$,

From Fig. 7 (a) and Fig. 7 (b), it can be concluded that parallel PV connected converter with MPPT control system gives better VR and proportional current sharing when two PV sources deliver same power.

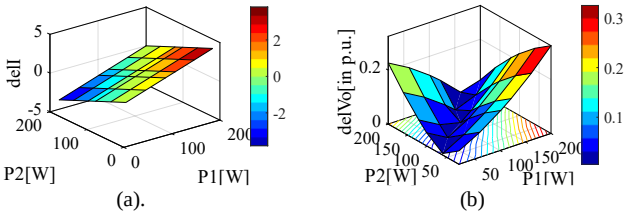

(a). (b)

Fig. 7. For variable PV power at non-MPPT mode (a) Current sharing ratio, (b) Output Voltage deviation.

In MPPT mode, the V_{MPP} point does not change much which is the input voltage of the converter. However, maximum power from the panel and current value changes with irradiation. Therefore, the voltage deviation like earlier case can be assumed to be less than 10% of 48 i.e. 4.8 V or in p.u. 4.8/48=0.1and the duty ratio range can be obtained using equation (10). The voltage deviation in p.u. is shown in Fig. 7 (b). From the voltage deviation in p.u. the duty ratio range can be determined which is dependent mainly on irradiation and the corresponding range is shown in Fig. 8 (a) -Fig. 8 (c).

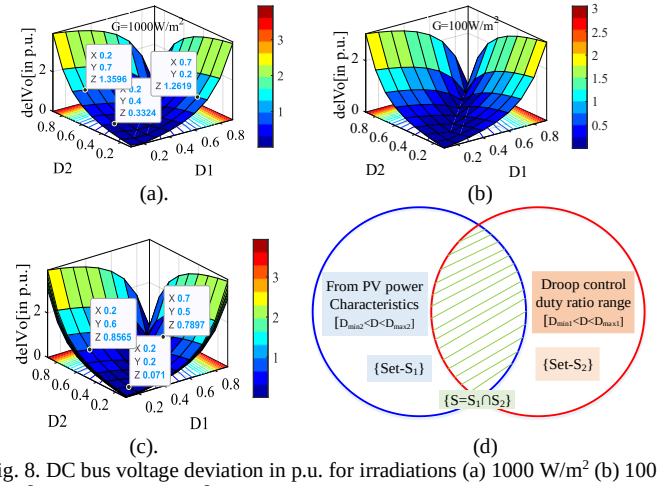

(a). (b) (c). (d)

Fig. 8. DC bus voltage deviation in p.u. for irradiations (a) 1000 W/m^2 (b) 100 W/m^2, (c) 1000-100 W/m^2, (d) Mapping of duty ratio.

$$\Delta v_{o\_nonMPPT} = \frac{P_{1max}}{I_{1min}} - \frac{P_{1min}}{I_{1max}} - [R_1 + R_{c1}][I_{1min} - I_{1max}] = \frac{P_{2max}}{I_{2min}} - \frac{P_{2min}}{I_{2max}} - [R_2 + R_{c2}][I_{2min} - I_{2max}] = \frac{P_{1max}}{I_{1min}} - \frac{P_{2min}}{I_{2max}} - [R_1 + R_{c1}]I_{1min} + [R_2 + R_{c2}]I_{2max} = \frac{P_{2max}}{I_{2min}} - \frac{P_{1min}}{I_{1max}} - [R_2 + R_{c2}]I_{2min} + [R_1 + R_{c1}]I_{1max} \quad (6)$$

This article has been accepted for publication in IEEE Journal of Emerging and Selected Topics in Power Electronics. This is the author's version which has not been fully edited and content may change prior to final publication. Citation information: DOI 10.1109/JESTPE.2024.3486554

$$\Delta v_{o\_MPPT} = \left[\frac{v_{1max}}{[1-D_1]CF_1} - \frac{v_{2min}}{[1-D_2]CF_2} - (1-D_1)CF_1 I_{1min}(R_1+R_{c1}) + (1-D_2)CF_2 I_{2max}(R_2+R_{c2})\right] \quad (10)$$

Due to nonlinearity in PV characteristics and MPPT mode restriction, a set of duty ratio i.e. S_1 (D_1<D<D_2) can be calculated to keep VR within 10%. Again, to incorporate change in droop coefficient, which control both VR and current sharing, another set of duty ratio i.e. S_2 (D_3<D<D_4) can be found. The common mapping between Set-S_1 and Set-S_2 as shown in Fig. 8 (d) is the operating duty ratio range. Therefore, for PV connected parallel system for successful droop control for proportional current sharing the duty ratio limitation is,

$$S = S_1 \cap S_2 \text{ and } R_c << R_{in}. \quad (11)$$

C. *Closed Loop Control with MPPT and Droop Coefficient Adjustment*

PV integrated parallel converter without and with MPPT control has major problems of VR and proportional current sharing under input power variations. Separate control along with MPPT is necessary to achieve better VR and current sharing. Internal impedance of converter and cable resistance affect the droop coefficient with increased loading as shown in Fig. 1. Droop control can modify the internal impedance of converter. Cable resistance also impacted on the resultant droop coefficient which is the addition of converter internal impedance to cable resistance. Cable resistance is almost constant and can be considered as a constant part of resultant droop coefficient. By keeping bus voltage constant, different cases are analyzed in terms of CSD. By assuming the zero-VR or stiff bus voltage (i.e. 1 p.u.), three different conditions arise considering two PV strings are in parallel. Fig. 9 (a) to Fig. (d) depicts the cases like,

(a) similar droop slopes with different short circuit current i.e. I_{SC1} and I_{SC2}.

(b) different droop slopes with similar short circuit current.

(c) different droop slopes with different short circuit current.

The expression for current sharing under constant DC link voltage is,

$$\Delta I = I_1 - I_2 = (m_2 - m_1)V_{MPP} + (I_{sc1} - I_{sc2}) \quad (12)$$

The absence of droop coefficient adjustment under a constant DC link voltage creates converter loading imbalance. This creates overburden or underutilization of PV integrated parallel converter as shown in Fig. 9 (a) and Fig. 9 (b).

Fig. 9 (d) shows the change in current sharing under small change in converter voltage or at non-zero VR. Applying the droop control method, VR problem can be resolved as shown the Fig. 10 (a). But this method has limitation as internal impedance variation range is narrow and the droop coefficient adjustment is not possible when cable resistance is large. So, cable resistance affects [27] VR and current sharing even though proper adjustment of droop coefficient is selected. The internal impedance of boost converter is

$$R_{in} = (1\text{-}D)^2 R_L \quad (13)$$

The condition to have valid droop controllability of the system for maintaining constant DC link voltage is,

$$\frac{R_{in}}{R_c} = \frac{(1\text{-}D)^2 R_L}{R_c} \geq 1 \quad (14)$$

PV sources are not stiff sources. Because of this accurate duty ratio control is not possible practically to achieve zero VR. By adjusting droop coefficient CSD can be minimized. Therefore, there is a tradeoff between CSD and zero VR. Fig. 10 (b) depicts the control block diagram of the proposed scheme. It looks like dual loop control where the inner loop is faster current mode and outer loop is slower voltage mode. Additionally, there is an adjustment in droop coefficient by finding the reference voltage. The droop coefficient needs to be variable for dynamic loading condition as shown in Fig. 10 (a). Dynamic variation of droop coefficient become complex under input voltage variation due to irradiation change.

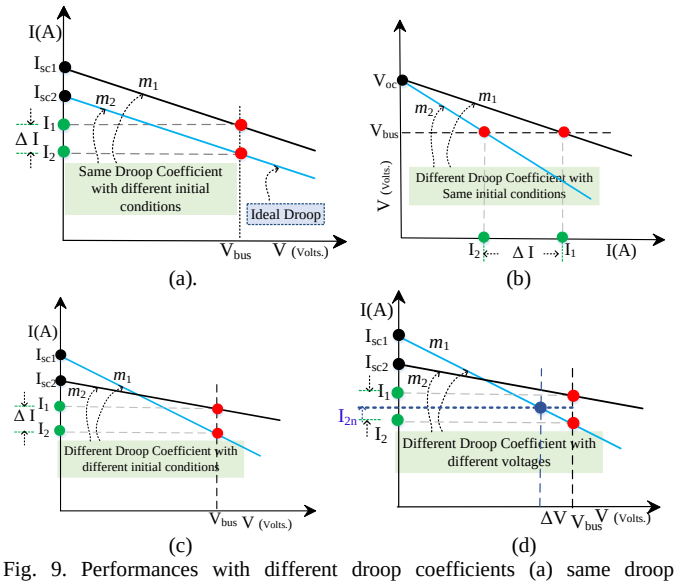

Fig. 9. Performances with different droop coefficients (a) same droop coefficient with different initial positions (b) different droop coefficients with same initial condition at constant bus voltage (c) different droop coefficients with different initial conditions (d) different droop coefficients with allowable voltage variation.

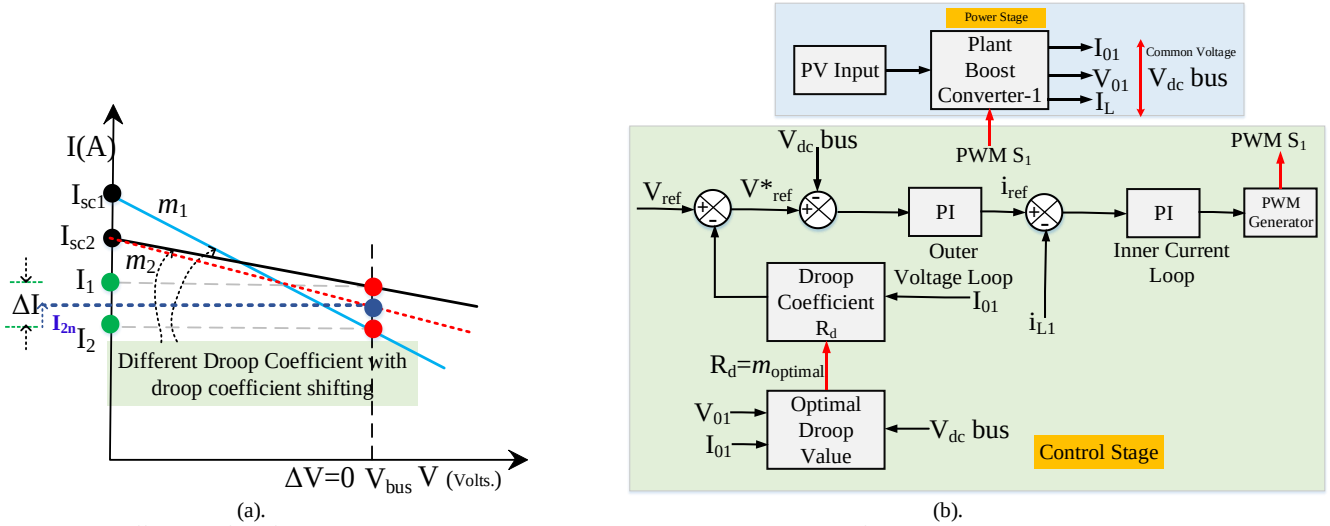

Fig. 10. (a) Droop coefficient shifting for enhanced regulation and load sharing (b) control block diagram of the proposed scheme.

This article has been accepted for publication in IEEE Journal of Emerging and Selected Topics in Power Electronics. This is the author's version which has not been fully edited and content may change prior to final publication. Citation information: DOI 10.1109/JESTPE.2024.3486554

The stable operating regions are very limited applying PI based dual loop control. Fig. 11 (c) and Fig. 12 (c) show the stable region for a typical PV tied boost converter where input voltage varies with perturbation of ± 10% and output constant voltage of 48V for 100W system. PSIM 9.1.1. Smart Control is used to determine the PI gain values of the parallel boost converter system for the DC Microgrid.

(a) Outer voltage loop gain plot including the PI Compensator: Switching frequency (f_{sw})=20 kHz, Crossover frequency = 117.454 Hz. Phase margin (PM)= 64.8649°. $\frac{v_{ref}}{v_o}$= 0.0520833, R_{11}(ohms) = 10kΩ, K_p = 1.40047, K_{int} = 197.436μ, R_2 = 14.0047 kΩ, C_2 = 14.0979 nF, f_z= 806.107 Hz and f_i = 1.12893 kHz. The gain and phase plot are shown in Fig. 11 (a) and Fig. 11(b) respectively. Voltage step response is shown in Fig. 11 (d).

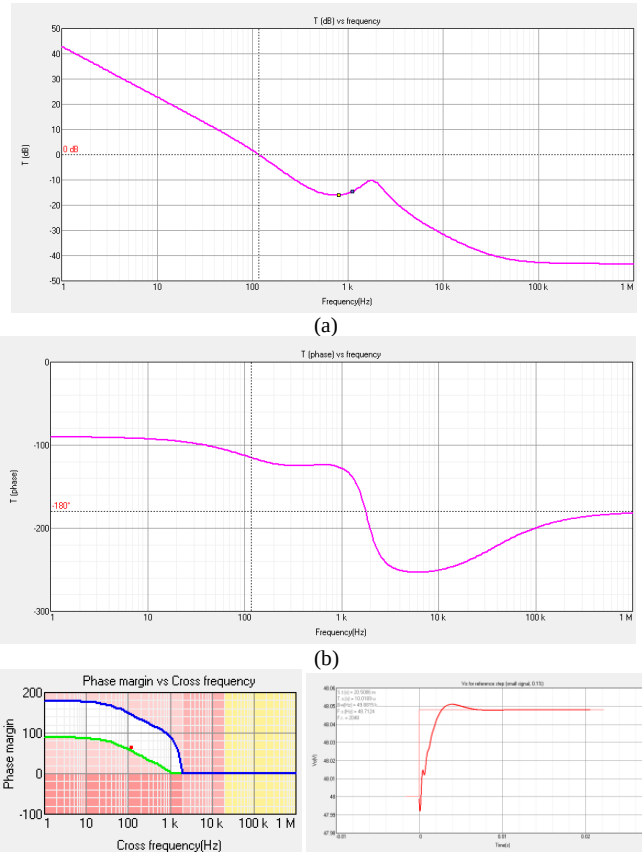

(a)

(b)

(c). (d)

Fig. 11. Outer voltage loop (a) gain plot (b) phase plot (c) Selection of PI value and (d) voltage step response.

(b) Inner current loop gain plot including the PI Compensator: K_p = 1.40047, K_{int} = 197.436 u, R_2 = 14.0047kΩ, C_2= 14.0979 nF, f_z = 806.107 Hz, f_i = 1.12893 kHz,
R_a = 9.10001 kΩ, R_b = 500Ω, P_a= 227.5 mW, P_b= 12.5 mW
Crossover frequency (Hz) = 1.995 kHz, Phase Margin= 30.66 Degree. The gain and phase plot are shown in Fig. 12 (a) and Fig. 12 (b) respectively. Current step response is shown in Fig. 12 (d).

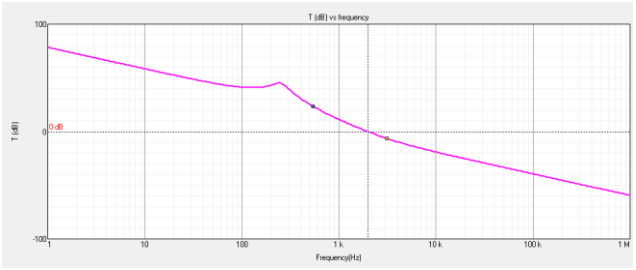

(a)

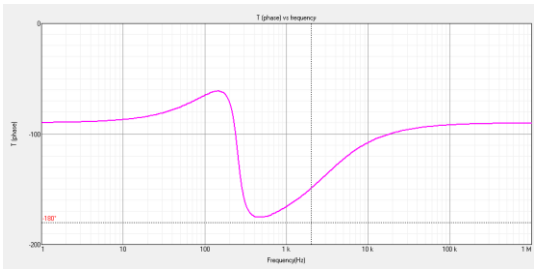

(b)

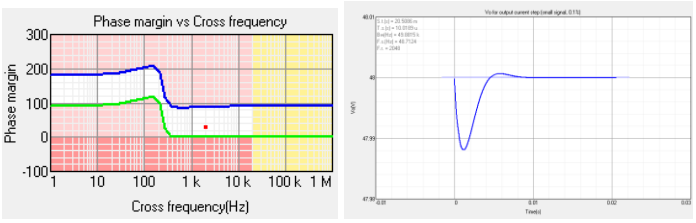

(c). (d)

Fig. 12. Inner current loop (a) gain plot (b) phase plot (c) Selection of PI value and (d) voltage response under step load change.

Overall closed loop gain and phase plot including inner current and outer voltage loop is shown in Fig. 13.

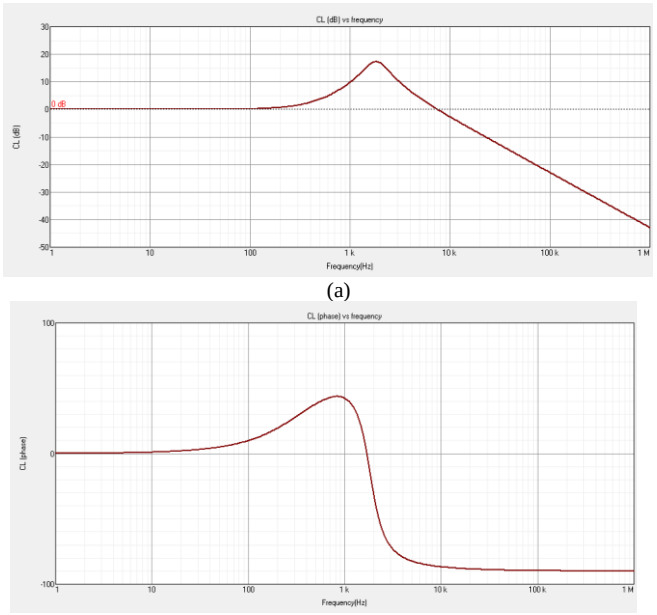

(a)

(b)

Fig. 13. Overall closed loop (a) gain plot (b) phase plot.

From Fig. 11 (d) and Fig. 12 (d), it is confirmed that DC link voltage can be fixed easily using droop control for many conditions like input voltage variation, step reference voltage variation and step load variation. However, the stability range is limited. The converter parameters and controller values are mentioned in Table-I.

Table-I
Boost Converter Parameters

Input Voltage	Output voltage	System Parameters	Controller value
Converter-1, 25-31V	48 V	L_1=500 μH, Inductor ESR r_l = 0.02Ω, C_o= 220 μF, Capacitor ESR r_c = 0.02Ω Cable resistance R_{c1}=100mΩ Droop coefficient variation= 0.1 to 0.37 Optimal droop coefficient=0.22 Watt=250 W	Switching frequency=20kHz Outer droop coefficient-based voltage loop PI value K_p = 1.40047, K_{int} = 197.436 μ Phase margin=64.86º Inner current loop PI value K_p = 1.40047, K_{int} = 197.436 μ Phase margin=30.66º

Converter-2, 25-31V	48 V	L_2=500 µH, Inductor ESR r_l = 0.02Ω, C_o= 220 µF, Capacitor ESR r_c = 0.02Ω Cable resistance R_{c2}=110mΩ Droop coefficient variation= 0.1 to 0.37 Optimal droop coefficient=0.22 Watt=250W	Switching frequency=20kHz Outer droop coefficient-based voltage loop PI value K_p = 1.40047, K_{int} = 197.436 µ Phase margin=64.86° Inner current loop PI value K_p = 1.40047, K_{int} = 197.436 µ Phase margin=30.66°

III. Proposed Sector-wise Droop Control

VR and CSD between power converters largely impacted by the voltage droop characteristics. The practical droop characteristics has nonlinear droop coefficient [13]-[15], [18]. Therefore, updating the droop coefficient as per its non-linearity in the control loop is essential. The resultant droop coefficient is,

$$R_{droop}=R_{in}+R_c \tag{15}$$

Where, $R_{in}=f_{in}(D,i_L,f_{sw})$ and R_C=Cable resistance. D=duty ratio, I_L=Load current, f_{sw}=switching frequency. Practical droop characteristics is shown in Fig. 14 (a).

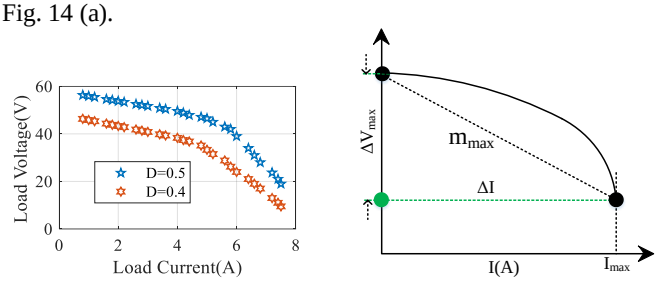

Fig. 14. Nonlinear droop characteristics

Using linear droop, the maximum droop coefficient (m_{max}) value can be derived as shown in Fig. 14 (b).

$$m_{max}=\frac{\Delta V_{max}}{I_{max}} \tag{16}$$

This m_{max} value is far from the actual droop coefficient thereby creating error in conventional droop-based VR and current sharing. For multiple parallel connected converter system,

$$V_{bus}=V_{ref}-m_i i_i \text{ and } V_{bus}=V_{ref}-m_k i_k \tag{17}$$

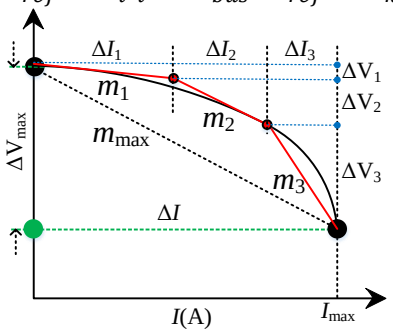

Fig. 15. Sector wise linear droop coefficient adjustment.

$$\text{Therefore, } \frac{m_i}{m_k}=\frac{i_k}{i_i}=\frac{R_i+R_{ci}}{R_k+R_{ck}}. \tag{18}$$

$R_{ci,k}$ is the cable resistance which is constant. Updating droop coefficient piecewise needs infinite sections to ideally match the exact nonlinear droop characteristics. For example, if three sections are considered as shown in the Fig. 15, the voltage and current deviation can be written as

$$\Delta V_{max}=\Delta V_1+\Delta V_2+\Delta V_3=\Delta I_1 m_1+\Delta I_2 m_2+\Delta I_3 m_3 \tag{19}$$

$$\text{And, } I_{max}=\Delta I_1+\Delta I_2+\Delta I_3 \tag{20}$$

Finding three variables from two equations needs one extra equation for solving or finding different droop coefficient. Similarly, for larger sections needs more droop coefficients values which needs more calculations. The extra equation can be from empirical relationship like ΔI_2=0.2 I_{max}. But this type of solution is system dependent and can't be generalised. Ratio based method is another alternative for finding different droop coefficient,

$$\Delta V_2=\mu_1\Delta V_1,\ \Delta V_3=\mu_2\Delta V_1 \tag{21}$$

$$\text{And } \Delta I_2=\gamma_1\Delta I_1,\ \Delta I_3=\gamma_2\Delta I_1 \tag{22}$$

$$\text{Therefore, } m_1:m_2:m_3=1:\frac{\mu_1}{\gamma_1}:\frac{\mu_2}{\gamma_2} \tag{23}$$

For n number of sections to track entire nonlinear droop curve the droop ratio is

$$m_1:m_2:m_3:\ldots\ldots:m_n=1:\frac{\mu_1}{\gamma_1}:\frac{\mu_2}{\gamma_2}:\ldots:\frac{\mu_n}{\gamma_n} \tag{24}$$

Now, by taking $\mu_1=\sqrt{k_1}$, $\mu_2=\sqrt{k_2}$ where k_1 and k_2 are the distinct positive integer constants. and similar values for γ_1 and γ_2 the entire voltage segment can be covered. But to implement these ideal large sections of droop coefficients requires advanced microcontroller. For example, TMS320F28379D DSP processor needs almost 24 cycle to execute a square root function and large number of calculations required to map entire droop curve using multiple droop coefficients. This problem is mainly addressed in this section where the entire droop region is divided into two main sections i.e. (a) Almost linear droop range (approximately 50% of I_{max}) (b) parabolic droop range as shown in Fig. 15.

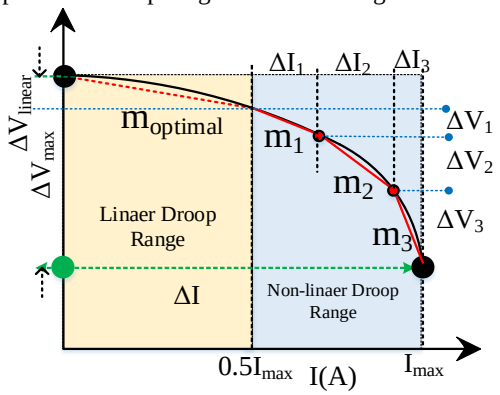

Fig. 16. Proposed sector wise droop characteristics.

For linear droop range only one optimal droop coefficient will be essential and for parabolic range maximum three droop sections will be required to achieve ease of control loop implementation as well as better performance in VR and CSD.

(a) **Linear Droop Range**:

The main objective of this region is to find optimal droop coefficient for multiple parallel connected converters. For simplicity in analysis the system shown in Fig. 4 is considered. The main objective is to find the optimal droop coefficient ($m_{optimal}$) so that the evident conduction loss as well as CSD can be minimized. Therefore, the objective should be minimum value of (a) the current difference of each converter i.e. $|I_1\text{-}I_2|$ in p.u. and (b) conduction loss [13] in p.u. due to converter internal impedance with cable resistance. Thus,

$$\text{Objective}_{linear}=min\{|I_1\text{-}I_2|+P_{cu}\} \tag{25}$$

$$\text{Where } P_{cu}=\{I_1^2R_{effective1}+I_2^2R_{effective2}\} \tag{26}$$

$$R_{effective1}=R_{in1}+R_{c1} \text{ and } R_{effective2}=R_{in2}+R_{c2} \tag{27}$$

The current difference i.e. $|I_1\text{-}I_2|$can be found out very easily by applying the KCL within two current loop paths.

$$I_1=\frac{V_1\text{-}V_o}{R_{in1}+R_{c1}},I_2=\frac{V_2\text{-}V_o}{R_{in2}+R_{c2}} \text{ and } V_o=[I_1+I_2]R_L \tag{28}$$

$$|I_1\text{-}pI_2|=\frac{1}{1+a}\left[\frac{V_1}{R_{effective1}}-\frac{V_2}{R_{effective2}}\right] \tag{29}$$

$$\text{Where, } a=\left[\frac{R_L}{R_{effective1}}-\frac{R_L}{R_{effective2}}\right], \text{ and } p=\left|\frac{1-a}{1+a}\right| \tag{30}$$

For a>0, then p<1 and again for a<0 then p>1. This helps to regulate the I_2 value and affects the CSD.

By varying the duty ratio of the converters, the internal impedance can be varied and thereby droop coefficient can be made variable.

This article has been accepted for publication in IEEE Journal of Emerging and Selected Topics in Power Electronics. This is the author's version which has not been fully edited and content may change prior to final publication. Citation information: DOI 10.1109/JESTPE.2024.3486554

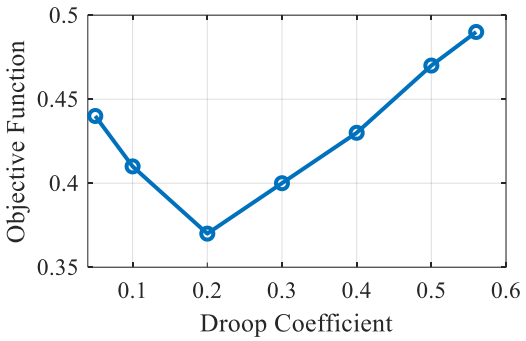

Fig. 17. Optimized droop coefficient for linear range operation.

Therefore, by changing the droop coefficient from minimum to maximum which mainly depends on converter internal impedance the objective function value in p.u. can be determined as shown in Fig. 17. Thus, for minimum objective function value the optimal droop coefficient can be obtained which is the constant value for a designed system. In this case this value is fixed in the linear droop region. Therefore, droop ratio modification is not necessary within 50% of I_{max} region as shown in Fig. 16. Variable internal impedance of individual converter using droop coefficient control is R_{in1} (R_{droop1}) and R_{in2} (R_{droop2}). The main objective of finding optimal droop coefficient to minimize CSD and to minimize copper loss without sacrificing the VR performance. Changing R_{droop} coefficient the minimum value of objective function is determined. The maximum droop coefficient range depends on the VR. In other words, it is the product of converter current and R_{droop}. If 5% voltage difference is allowed and rated current of the converter is 10 A, then the product of droop coefficient and rated current should be less than 2.4V (48X0.05=2.4V). This guides the range of R_{droop}. After that optimal value is calculated by minimalizing the objective function. The operating droop coefficient is 0.1 to 0.37. The optimal value is 0.22.

(b) **Extended Non-linear Droop Range**:

50% of the loading range is controlled by the optimal droop coefficient which confirms the better current sharing and VR performance without increasing the calculation complexity. But extended loading range which is greater than 50% of converter capacity is decided by the allowable voltage deviation i.e. ΔV_{max}. The extended range is decided by the I_{max} and ΔV_{max}. Empirically, through experiment on 250W and 1.5kW separate boost converter it is found that the extended range can be maximum reach to 65%-70% of the maximum current carrying capability of individual converter without sacrificing the bus voltage deviation greater than ±3%. If more deviation is allowed i.e. ±5% then more loading i.e. $0.8I_{max}$ can be performed. However, this region is excessively nonlinear and prone to deviate from allowable VR i.e. ±5%.

In this article, between $0.5I_{max}$ to $0.7I_{max}$ three sections of droop coefficient is considered to reduce the calculation complexity and performance improvement. The method is explained in equation (24). By taking $\mu_1 = \sqrt{k_1}, \mu_2 = \sqrt{k_2}$.Generally, k_2>k_1 is considered to map the extended nonlinear droop range accurately. To apply the proposed method, it is very important to understand the output impedance of the power converter which is variable through duty ratio. Droop coefficient can be updated by managing the output impedance which is required for extended range of droop operation. As, the cable resistance is uncontrolled and constant. For this analysis its value is small compared to output impedance of the converter i.e. R_{in}>R_c. For other condition when R_c>R_{in} variable resistance converter is required which is not the case for current analysis. By changing the droop coefficient converter output impedance also changes and it can be good for VR and current sharing as discussed but another major issue is the system stability. As per Middlebrook absolute stability criteria [28]-[31] the converter output impedance (Z_o) should be less than load impedance (Z_i) i.e. Z_i>>Z_o. But sometimes even though the condition is violated system remains stable. Therefore, impedance-based stability determination method is suitable as this do not need accurate parameter information and impedance measurement is performed by the network analyser.

(i) Impedance measurement of droop-controlled converter using network analyser:

The output impedance (Z_o) is a critical and network analyser-based impedance measurement method [34] is adopted in this work.

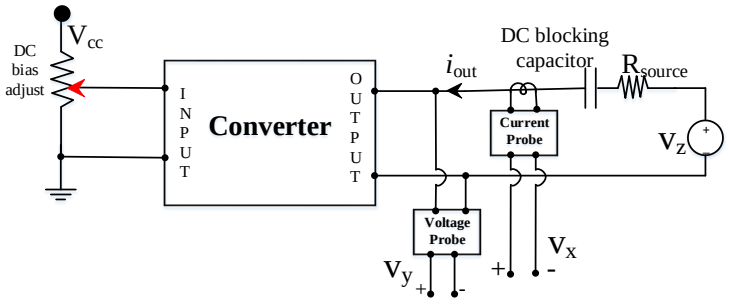

Fig. 18. Network analyzer-based impedance method.

The measurement procedure is shown in Fig. 18 where V_x and V_y are measured current and voltage. The block diagram of droop-controlled boost converter system is shown in Fig. 10 (b). The output impedance transfer function of the droop-controlled system using small signal analysis is mentioned in equation (28) which is derived from the block diagram shown in Fig. 19.

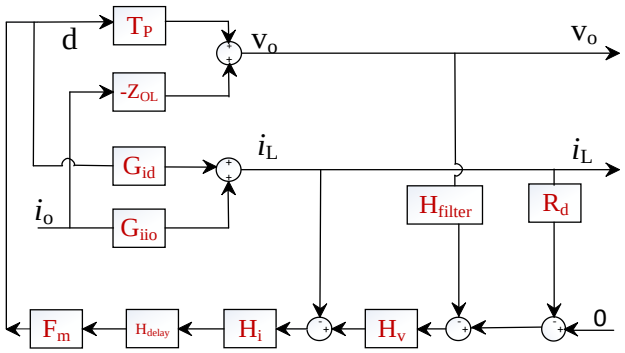

Fig. 19. Transfer function model of droop-controlled boost converter.

$$z_o = -\frac{v_o}{i_o} = \frac{z_{o\_oL} + \frac{T_P G_{iio}}{G_{id}}}{1 + \frac{T_P H_v H_{filter}}{(R_d H_v + 1) G_{id}}} \quad (28)$$

Where $Z_{0\_OL} = \frac{R_L r_c (s + 1/r_c C)(s + r/L)}{(R_L + r_c)(s^2 + 2zeta w_o s + w_o^2)}$ [4].

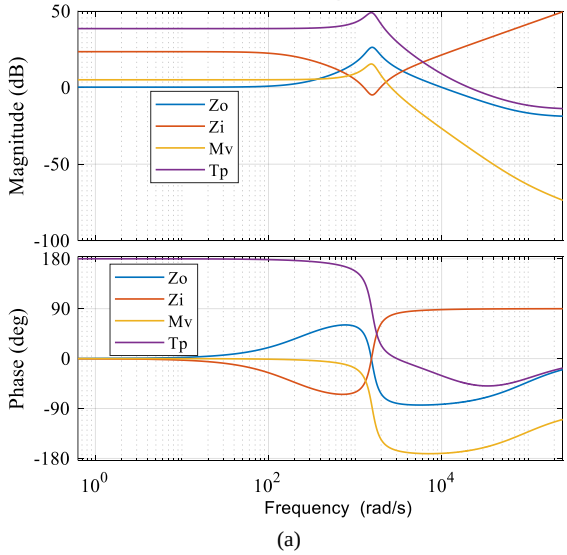

(a)

This article has been accepted for publication in IEEE Journal of Emerging and Selected Topics in Power Electronics. This is the author's version which has not been fully edited and content may change prior to final publication. Citation information: DOI 10.1109/JESTPE.2024.3486554

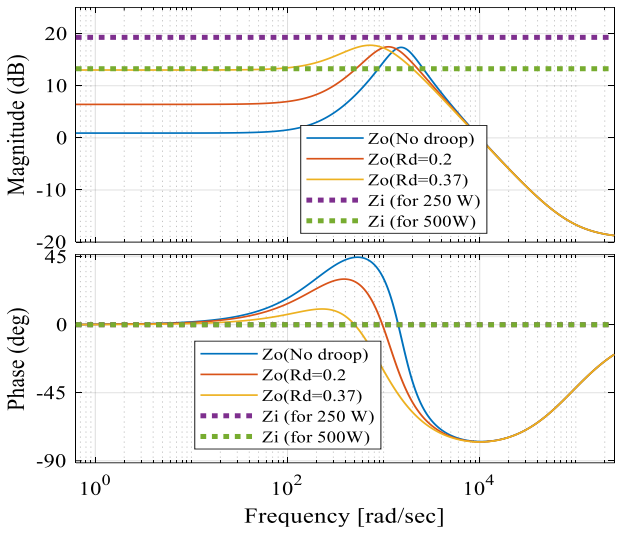

Fig. 20. (a) Voltage loop, output and input impedance gain without droop control, (b) Output impedance gain with droop coefficient variations.

It is important to find output impedance after applying the droop control as impedance-based method is accurate for stability determination in closed loop system. The open loop transfer function gain of like system gain i.e. $\frac{v_o}{v_{in}} = M_v$, voltage loop gain $\frac{v_o}{d} = T_p$, output impedance $\frac{v_o}{i_o} = z_o$and input impedance $\frac{v_{in}}{i_{in}} = z_i$ $G_{id} = \frac{i_L}{d}$, $G_{ii0} = \frac{i_L}{i_o}$, using small signal analysis is shown in Fig. 20 (a). By varying the droop coefficient, the variations of the output impedance are shown in Fig. 20 (b).

For stability analysis two widely accepted methods are (a) state space analysis and (b) impedance-based analysis. In state space analysis stability mainly depends on the eigenvalues of the system's state space equation. For this complete knowledge of all converter parameters is necessary. However, these parameters are not always available and finding stability using this technique is moderately difficult. On the other hand, using impedance-based criteria is simple and only needs measurements of impedance using black box model. To confirm the stability using Middlebrook criteria [29], the magnitude of the converter output impedance (Z_o) must be much smaller than the magnitude of the load input impedance (Z_i) [30]-[31]. $|Z_o| \ll |Z_i|$. Therefore, the impedance ratio [28] at point of common coupling is, $T_m = \frac{Z_o}{Z_i}$, The desired stability margins of T_m is to define a forbidden region for the polar plot of T_m as shown in Fig. 21.

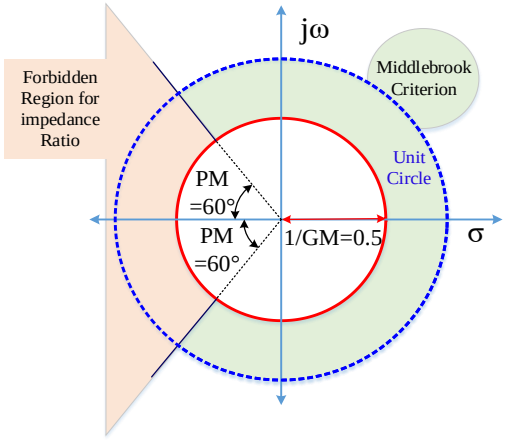

Fig. 21. Polar plot of T_m

The forbidden region in the polar plot is formed by assuming phase margin of 60º and gain margin of 6dB [28]. The polar plot of T_m does not enter the forbidden region confirm stability of the system (not possible for the polar plot of T_m to encircle the critical point (-1, j0)).

If T_m crosses a negative portion of the real axis the magnitude of T_m will be less than 0.5 (at least 6dB of gain margin) and when it crosses the unit circle the phase of T_m will always maintain 60º phase margin. The impedance-based method does not need all converter parameters since the converter input and output impedances can be measured using network analyzer. To use impedance-based criteria the modelling and measurement of output impedance of droop-controlled converters is critical. In the proposed work there are only four droop coefficients (one optimal $m_{optimal}$, three piecewise m_1, m_2 and m_3) and the measurement is not difficult like other proposals where continuous droop coefficient adjustment is required.

For 250W, Z_i= 2304/250=9.16Ω, in dB scale, Z_i=20log 9.216 dB=19.290 dB and for 500W, Z_i= 2304/500=4.608Ω, in dB scale, Z_i=20log 4.608 dB=13.27 dB. Both plots are shown in Fig. 20. From Fig. 20 (b) it is clear, for 250W and for droop resistance R_d=0.2 the input impedance is greater than the output impedance for wide bandwidth. Similarly, for 500W and for droop resistance R_d=0.2 the input impedance is greater than the output impedance upto 400rad/sec. For other droop resistance R_d=0.37 the output impedance is greater than input impedance at 500W. Thus, in this work droop resistance, R_d=0.22 is selected which improves both current sharing performance and stability. This also ensures optimal CSD and conduction loss minimization.

(ii) Stability analysis with variable resistance load and CPL:

For ELVDC system, if load is dominated by resistance, then droop control based internal impedance will be always less than the load impedance Z_i>>Z_o. For lightly loading or no-load condition boost converter will operate based on dummy local load otherwise boost converter will be unstable. Therefore, for variable loading in ELVDC microgrid if dominated by the resistance there will not be stability issues except deviation in allowable VR. With the current proposal on droop resistance variation based on sector wise technique not only confirms good VR but it also offers extended range of operation without increasing computation complexity. The main problem creates when connected constant power load or mixed load i.e. both variable resistance as well as constant power load. For a constant power load, the reflected resistance on the input side becomes negative and droop resistance needs to be infinite to make system stable, which is not practically possible. Therefore, for constant power loading the stability margin is very less and depending heavily on filter impedance. For larger value of filter capacitor system [32] stability margin can be enhanced for constant power loading. The compromise in that case will be on cost, bulkiness, and size of the capacitor. But, if Z_i>>Z_o can be maintained for mixed loading i.e. for both variable resistance and CPL [33] then stability margins do not depend on the droop coefficient variation.

IV. Experimental Validation And Results

PSIM 9.1.1. is used for modelling and applying the proposed sector wise optimized droop control for 1.5 kW ELVDC microgrid system.

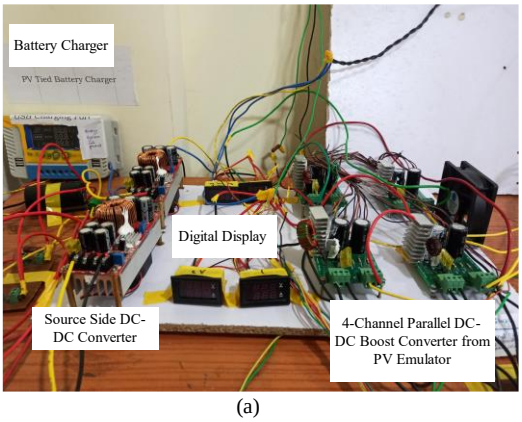

(a)

This article has been accepted for publication in IEEE Journal of Emerging and Selected Topics in Power Electronics. This is the author's version which has not been fully edited and content may change prior to final publication. Citation information: DOI 10.1109/JESTPE.2024.3486554

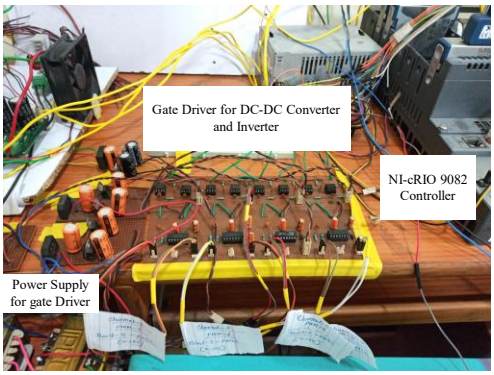

(b)

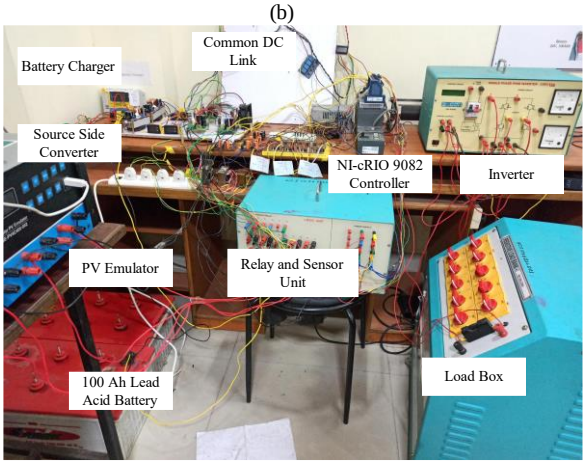

(c)

Fig. 22. (a) Four PV emulator integrated, and two physical PV panel connected converter power circuit (b) Driver circuit (c) Overall designed system controlled by NI-cRIO 9082.

The designed prototype hardware system is shown in Fig.22 (a), Fig. 22 (b) and Fig. 22 (c). The theoretical findings of the system under load change and irradiation change without controller as well as droop-based controller is simulated. The simulation parameters are shown in Table-II.

Table-II
1.5 kW ELVDC System Parameter

Irradiance(w/m^2)	100-1000W/m^2 with variations of 200W/m^2		
Physical PV panel and Emulator	250WX2=500W, 4-channel PV Emulator of 1.5kW capacity (Max)		
Boost Converter-2nos	Vin=25V-31V	Vo=48V	F_{sw}=20kHz
Load	Constant Load=500W	Variable load=250W-300W-500W	Perturbance=100W
Control	Inner current mode	Outer voltage mode (resistive divider)	Optimal sector wise droop control
Embedded Controller	NI-cRIO 9082		
Sensors and Driver	NI-9225 for voltage sensor, NI-9227 for current sensor, IR2110 for MOSFET driver, 6N137 opt coupler for optical isolation.		

Test-1: *Performance at open loop control and non-MPPT mode*: For small change in Load of ±100W and base load 400W, proportional current sharing ratio is good and DC Link voltage deviation is small as shown in Fig. 23 (a)-Fig. 23 (d).

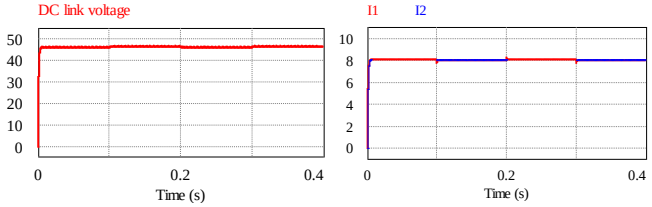

(a). (b)

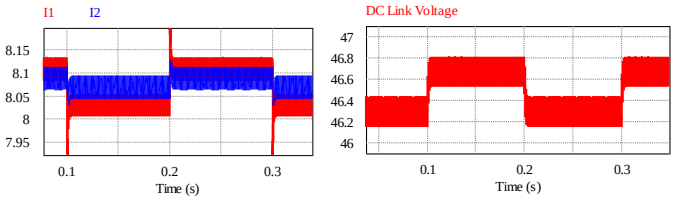

(c). (d)

Fig. 23. (a) DC link voltage (b) current sharing (c) current sharing difference (d) voltage deviation.

When load change is steep i.e. ±250W, both DC link voltage deviation is large and proportional current sharing performance also affected as shown in Fig. 24 (a) and Fig. 24 (b).

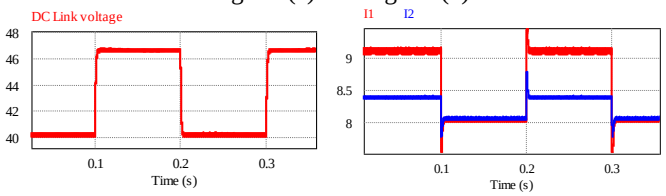

(a). (b)

Fig. 24. Load change (±250W) effect (a) DC link voltage (b) current sharing.

Application of MPPT control gives the similar response under different irradiance for constant loading. To improve the regulation and proportional current sharing, droop control is implemented along with MPPT by keeping the low value of cable resistance to satisfy the equation (14).

Test-2: *Load variation at fixed irradiation with droop and MPPT control.*

After applying proposed droop control with MPPT the regulation performance is improved as shown in Fig. 25 (a)-Fig. 25 (f).

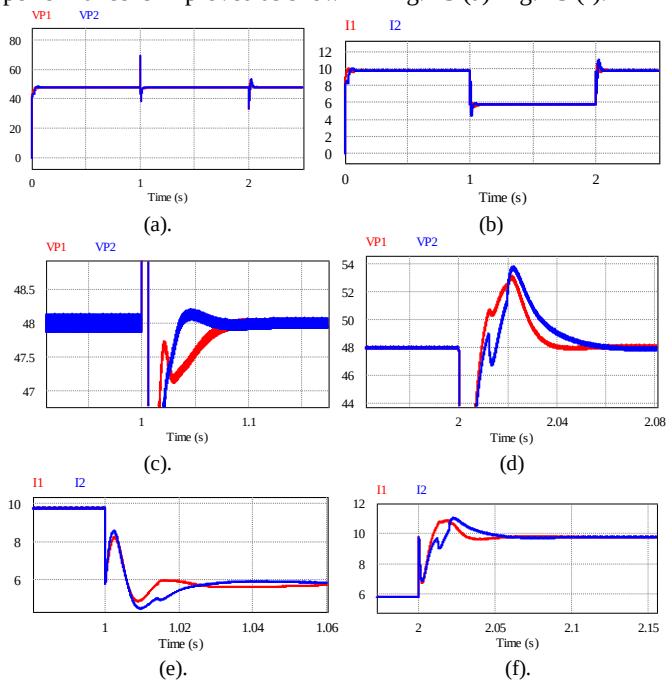

(a). (b)

(c). (d)

(e). (f)

Fig. 25. (a) DC link voltage (b) current sharing (c) & (d) voltage difference (e) & (f) current difference for load variation with MPPT and droop control.

Cable resistance affects the current sharing performance of two individual PV string. Thus, VR and proportional current sharing occurrence depends on the boundary conditions determined by the internal impedance of the converter and cable resistance. Large cable resistance makes stable DC link voltage (Fig. 26 (a)), but current sharing fails as shown in Fig. 26 (b) and Fig. 26 (c). The proposed control improves VR and equal current sharing. The first testing is performed with negligible cable resistance where loading is increased from 25% to 50%. The DC link voltage is stable with changeover transient is 1.2V/sec.

This article has been accepted for publication in IEEE Journal of Emerging and Selected Topics in Power Electronics. This is the author's version which has not been fully edited and content may change prior to final publication. Citation information: DOI 10.1109/JESTPE.2024.3486554

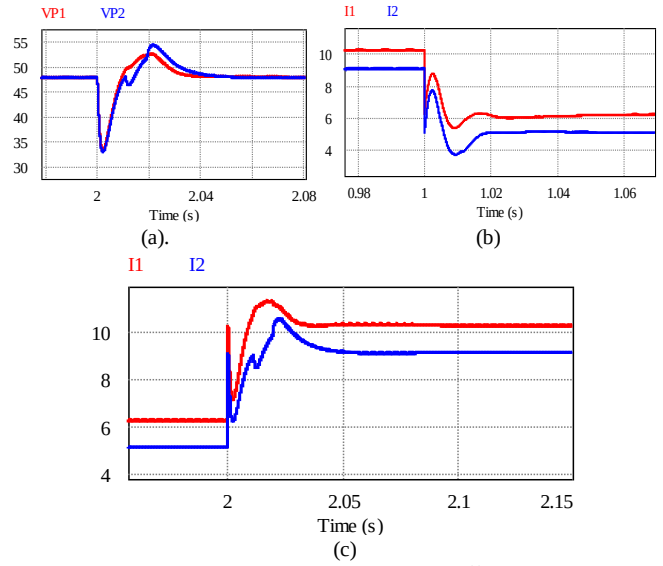

Fig. 26. (a) DC link voltage (b) & (c) current sharing difference.

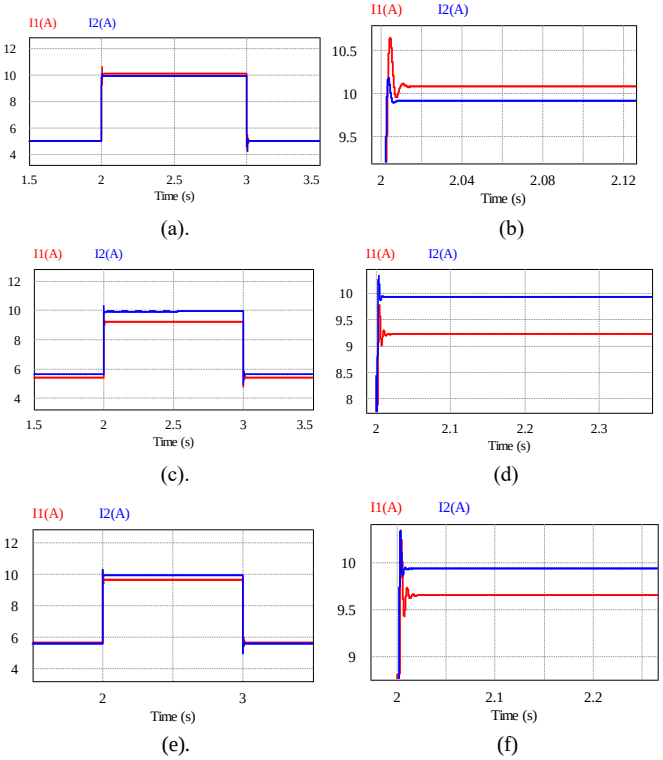

Fig. 27. Current regulation performance at enhanced loading (a)-(b) [25] (c)-(d) [13], [14] (e)-(f) proposed.

In the simulation study nonlinear droop control [13]-[14] and adaptive discrete droop coefficient [25] are compared to proposed control method. For each case 50% loading is increased at 2 sec which makes the boost converter operation in nonlinear droop range. The current regulation performance of [25] is shown in Fig. 27 (a) -Fig. 27 (b). The results for [13] and [14] are shown in Fig. 27 (c) and Fig. 27 (d) which shows poor performance compared to [25] at enhanced loading. At the same condition current proposal is tested provides better results compared to [13]-[14] as shown in Fig. 27 (e) and Fig. 27 (f).

The current sharing performance is also improving from two different boost converter as shown in Fig. 28 (a). The cable resistance plays an important role for settling time of converter load current under load variation. For larger cable resistance the settling time of converter output current increases with conventional droop control. But using the current proposed optimal droop control the current changeover slope increases as shown in Fig. 28 (b).

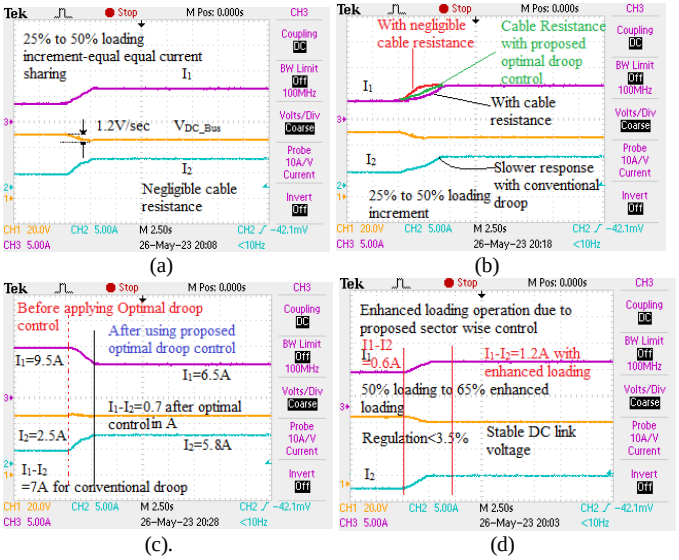

Fig. 28. (a) Voltage regulation and current sharing performance with negligible cable resistance (b) Current sharing slope compensation using proposed sector-wise control (c) & (d) performance improvement of current sharing using proposed droop control.

Using proposed control, the CSD between converters also reduces which confirms proportional load sharing. For constant loading i.e. at 50% loading of individual converter the converter-1 shares 9.5A current and converter-2 shares 2.5A current which DC link voltage is stable 48V. Thus, using conventional droop control the CSD is 7A approximately.

Table-III
Comparative Study

Type of Control with reference	Optimal droop coefficient for loss minimization	Enhanced loading Capability	Computation burden and complexity	Voltage Regulation [VR]	Current sharing difference
Conventional droop Control					
Droop coefficient adjustment.[6]	No	No	Low	Poor	Increased with enhanced loading.
Fixed droop coefficient change. [10].	No	No	Moderate. for calculating K_1 and K_2 coefficient and storing in look up table	Moderate	Moderate

Non-Linear Droop Control					
High droop gain (HDG) method [11]	No	Moderate	Moderate	Good	Poor at intersection between linear and non-linear droop curve
Polynomial droop curve (PDC) method [12]	No	Yes	High	Good. However, VR performance is poor near rated loading condition.	Good current sharing performance. However, Number of droop segments should be odd to maintain symmetry.
Polynomial droop curve with voltage compensation (PDCVC). [13]	No	Yes	High	Good. Better voltage regulation at high loading condition.	Due to asymmetry the current sharing performance is poor near light loading condition.
Curve fitting method. [14]	No	Yes	High	Good performance at heavy loading condition	Better performance in heavy loading condition. However, at light loading condition the performance is like HDG.
Lyapunov control [15]	No	Yes	High	Good performance with implementation complexity. Heavily depends on control parameter selection.	Good performance for both resistive load and CPL.
Data driven non-linear droop control. [16]	No	Yes	High	Good. However, highly depends on data accuracy and mapping of non-linear graph (elliptical)	Good. Highly depends on data accuracy and mapping of non-linear graph (elliptical).
Current-Mode Droop Control [17]	No	Yes	High	Like $i_{dc} - v_{dc}^2$ approach. Good performance. However, the operation is limited by high droop gains.	Slightly improved current sharing accuracy in multi-source operation. Current sharing performance is poor while adapting load variation under dynamic condition.
Piecewise Droop Control					
Distributed piecewise droop control [20]-[21]	No	Yes	Moderate	Good performance. However, droop coefficient value depends on K_n parameter, which is complex to find, and the approach is like offset voltage addition. There is no guideline for three major sections.	Improved current regulation. However, the performance is poor during dynamic load change due to the fact of improper characteristics fitting.
Piecewise linear formation of droop strategy (PLFDS) [19]	No	Yes	High	Good performance. However, tuning of different sections depends on loading and calculation is complex. This technique is not good for online application.	Load current sharing is proportional and sharing error is less.
Multi-Section piecewise droop control [18]	No	Yes	High	Good performance but excessive section to fit droop curve provides slow response under dynamic condition. The number of sections depends on the size of the converter.	There is a problem of system oscillation. The current sharing performance is good under heavy load. However, the performance is poor at light load condition.
Other hybrid Method					
ANN based droop coefficient control. [22]	No	Yes	Excessively high	Good performance. However, the method is system dependent as training is done through offline method. On a different system training data may not converge and hence not a reliable solution for primary control.	Current sharing performance is also good. However, there is problem of oscillation at a local point.
Sliding mode adaptive droop control [23]	No	Yes	High	Good performance. However, fuzzy optimizer function is again depending on membership function and difficult to obtain considering converter parameter, cable resistance and PV power variation.	Current sharing performance is limited at light load condition.

Adaptive Discrete Piecewise Droop Control [25]	No	Yes	High	Performance is good and promising.	Current sharing performance is also better.
Proposed Sector wise droop control	Yes	Yes	Less complexity and easy to implement	Voltage regulation is <3.5% up to 65% loading.	Current sharing difference is in the range of 2-3%

However, after implementing optimal sector wise droop control in NI-cRIO-9082 embedded controller the performance betterment can be seen in Fig. 28 (c), where CSD reduces to 0.7A. Using proposed control, the stability range of DC link voltage is enhanced with variable resistive load. The achieved regulation is below 3.5% at this condition. However, with enhanced loading the CSD increases since under this condition converter enters nonlinear range of droop characteristics as shown in Fig. 28 (d). The performance betterment using proposed control compared to other solution is mentioned in Table-III and Table-IV.

Table-IV
Performance Comparison using Proposed sector-wise droop control.

	Proposed	[7]	[13]
Current Sharing Difference (I_1-I_2) (hardware)	2-3%	58%	8%
Voltage regulation (Hardware)	<3.5% with 65% loading For parallel boost	<5% For parallel buck	<2% For parallel buck
Computation Burden and Complexity	Less	Less	More
No of communication Channel	$n(n\text{-}1)$	$n(n\text{-}1)$	n
Enhanced Loading	In the current solution enhanced loading operation is possible maintaining DC link voltage.		

VI. Conclusion

In this work, initially the performance of voltage regulation and current sharing on PV integrated two parallel boost converters in ELVDC is tested without MPPT and closed loop control. The current sharing and voltage regulation are within 5% when load variation is nearer to converter output ports and irradiation variation is negligible. However, this system has major problem of underutilization of available power due to non-MPPT operation. Voltage regulation and current sharing performance becomes worse for a condition when load nearer to one converter and remote to another converter. Therefore, MPPT with droop control is necessary where it has been established that voltage regulation and current sharing performance can't be improved simultaneously. Non-linear droop characteristics further degrades the performance. Therefore, increased loading operation from each converter is not possible to maintain DC link voltage within limit while maintaining current sharing difference to a minimum value. In this current proposal, sector-wise droop control is proposed where entire region of droop characteristics is divided into two main sections. The optimal droop coefficient operation in linear region reduces the requirement of continuous modification of droop coefficient and it reduces the calculation complexity. Optimal droop coefficient ensures minimum current sharing difference i.e. 2-3% for up to 50% of individual converter loading capacity. The second section of droop characteristics is nonlinear where three small linear sections are made to fit the droop curve. This region guarantees enhanced loading operation up to 65%-70% of capacity without sacrificing voltage regulation and current sharing difference. However, in this region current sharing difference increases to 4.5% which is reasonable when operating loadability range is concerned in ELVDC microgrid. This mixed model of operation performs well for variable resistive load.

Appendix-I

Let power sharing ratio, $\mu_p = \frac{P_1}{P_2}$,

The current sharing ratio,

$$\frac{I_1}{I_2} = \frac{P_1}{P_2} \times \frac{V_2}{V_1} = \mu_p \frac{[v_o + I_2(R_2 + R_{c2})]}{[v_o + I_1(R_2 + R_{c2})]} = \mu_p \frac{[(I_1 + I_2)R_L + I_2(R_2 + R_{c2})]}{[(I_1 + I_2)R_L + I_1(R_2 + R_{c2})]} \quad \text{I.1}$$

By simplifying,

$$\left(\frac{I_1}{I_2}\right)^2 (R_1 + R_{c1} + R_L) + \frac{I_1}{I_2}(1 - \mu_p)R_L - \mu_p(R_2 + R_{c2} + R_L) = 0 \quad \text{I.2}$$

$$\frac{I_1}{I_2} = \frac{-(1-\mu_p)R_L \pm \sqrt{(1-\mu_p)^2 R_L^2 - 4 \times (R_1 + R_{c1} + R_L)\left(-\mu_p(R_2 + R_{c2} + R_L)\right)}}{2 \times (R_1 + R_{c1} + R_L)}$$

$$\frac{I_1}{I_2} = -x \pm y \quad \text{I.3}$$

Where,

$$x = \frac{-(1-\mu_p)}{2(1 + \frac{R_1 + R_{c1}}{R_L})}, y = \sqrt{\mu_p \frac{(R_2 + R_{c2} + R_L)}{(R_1 + R_{c1} + R_L)} + \left[\frac{(1-\mu_p)}{2(1 + \frac{R_1 + R_{c1}}{R_L})}\right]^2}$$

The maximum value of common DC link voltage is v_{omax},

$v_{omax} = v_{1max} - I_{1min}(R_1 + R_{c1})$, where v_{1max} is PV panel-1 maximum voltage, I_{1min} is minimum current from PV panel-1.

$$v_{1max} = \frac{P_{1max}}{I_{1min}}, v_{1min} = \frac{P_{1min}}{I_{1max}}, \quad \text{I.4}$$

Similarly for PV panel 2, $v_{omax} = v_{2max} - I_{2min}(R_2 + R_{c2})$

where, v_{2max} is PV panel-2 maximum voltage, I_{2min} is minimum current from PV panel-2.

$$v_{2max} = \frac{P_{2max}}{I_{2min}}, v_{2min} = \frac{P_{2min}}{I_{2max}}, \quad \text{I.5}$$

$$v_{omax} = v_{1max} - I_{1min}(R_1 + R_{c1}) = v_{2max} - I_{2min}(R_2 + R_{c2})$$

$$v_{omin} = v_{1min} - I_{1max}(R_1 + R_{c1}) = v_{2min} - I_{2max}(R_2 + R_{c2})$$

From these equations the DC link voltage deviations ($\Delta v = v_{omax} - v_{omin}$) for both non-MPPT and MPPT mode are derived which are mentioned in equation (5) and equation (9) respectively. The non-ideality factor of the boost converter is denoted by CF.

$$CF_i = 1 + \frac{v_d}{v_{sd}} + \frac{D_i r_{ds} + [1 - D_i] r_d + r_l}{[1 - D_i]^2 R_L}, \quad \text{I.6}$$

Where, v_d is diode forward voltage, v_{sd} is switch voltage, r_{ds} is MOSFET on-state resistance, r_d is the diode forward resistance, r_l is the ESR of the inductor, R_L is the load resistance and D_i is the operating duty ratio of the i^{th} boost converter.

References

[1] F. Blaabjerg, Z. Chen, and S. B. Kjaer, "Power electronics as efficient interface in dispersed power generation systems," *IEEE Trans. Power Electron*., vol. 19, no. 5, pp. 1184–1194, Sep. 2004

[2] M. Farrokhabadi et al., "Microgrid stability definitions, analysis, and examples," *IEEE Trans. Power Syst*., vol. 35, no. 1, pp. 13–29, Jan. 2020

[3] J. Hu, Y. Shan, K. W. Cheng and S. Islam, "Overview of Power Converter Control in Microgrids—Challenges, Advances, and Future Trends," in *IEEE Transactions on Power Electronics*, vol. 37, no. 8, pp. 9907-9922, Aug. 2022.

[4] M. Kazimierczuk, Pulse-Width Modulated DC–DC Power Converters. Hoboken, NJ, USA, John Wiley, 2008.

[5] L. Xu and D. Chen, "Control and operation of a dc microgrid with variable generation and energy storage," *IEEE Trans. Power Del*., vol. 26, no. 4, pp. 2513–2522, Oct. 2011

[6] C. Jin, P. Wang, J. Xiao, Y. Tang, and F. H. Choo, "Implementation of hierarchical control in DC microgrids," *IEEE Trans. Ind. Electron*., vol. 61, no. 8, pp. 4032–4042, Aug. 2014.

[7] J. Rajagopalan, K. Xing, Y. Guo, F. Lee, and B. Manners, "Modeling and dynamic analysis of paralleled dc/dc converters with master-slave current sharing control," in *Proc. IEEE 11th Annu. APEC Conf*., vol. 2, Mar. 1996, pp. 678–684.

[8] M. Ashourloo, A. Khorsandi and H. Mokhtari, "Stabilization of DC microgrids with constant-power loads by an active damping method," *4th Annual International Power Electronics, Drive Systems and Technologies Conference*, Tehran, Iran, 2013, pp. 471-475.

[9] J. M. Guerrero, J. C. Vasquez, J. Matas, L. G. de Vicuna and M. Castilla, "Hierarchical Control of Droop-Controlled AC and DC Microgrids—A General Approach Toward Standardization," in *IEEE Transactions on Industrial Electronics*, vol. 58, no. 1, pp. 158-172, Jan. 2011.

[10] J.-W. Kim, H.-S. Choi, and B. H. Cho, "A novel droop method for converter parallel operation," *IEEE Trans. Power Electron*., vol. 17, no. 1, pp. 25–32, Jan. 2002.

[11] B. T. Irving and M. M. Jovanovic, "Analysis, design, and performance evaluation of droop current-sharing method," in *Proc. IEEE Appl. Power Electron*. Conf., New Orleans, LA, USA, Feb. 2000, vol. 1, pp. 235–241.

[12] F. Chen, R. Burgos, D. Boroyevich, and W. Zhang, "A nonlinear droop method to improve voltage regulation and load sharing in dc systems," in *Proc. Int. Conf. DC Microgrids*, Atlanta, GA, USA, Jun. 2015, pp. 45–50.

[13] P. Prabhakaran, Y. Goyal, and V. Agarwal, "Novel nonlinear droop control techniques to overcome the load sharing and voltage regulation issues in DC microgrid," *IEEE Trans. Power Electron*., vol. 33, no. 5, pp. 4477– 4487, May 2018.

[14] Y. Zhang, X. Qu, M. Tang, R. Yao and W. Chen, "Design of Nonlinear Droop Control in DC Microgrid for Desired Voltage Regulation and Current Sharing Accuracy," in *IEEE Journal on Emerging and Selected Topics in Circuits and Systems*, vol. 11, no. 1, pp. 168-175, March 2021.

[15] Q. Xu, C. Zhang, C. Wen, and P. Wang, "A novel composite nonlinear controller for stabilization of constant power load in dc microgrid," *IEEE Trans. Smart Grid*, vol. 10, no. 1, pp. 752–761, Jan. 2019.

[16] S. Sharma, V. M. Iyer and S. Bhattacharya, "An Optimized Nonlinear Droop Control Method Using Load Profile for DC Microgrids," in *IEEE Journal of Emerging and Selected Topics in Industrial Electronics*, vol. 4, no. 1, pp. 3-13, Jan. 2023.

[17] Y. Chen, C. Yang, J. Li, J. Chen and F. Gao, "A Modified Current-Mode Droop Control Scheme for Building-Scale DC Microgrids," *2023 IEEE 2nd International Power Electronics and Application* Symposium (PEAS), Guangzhou, China, 2023.

[18] Hailu and J. A. Ferreira, "Piece-wise linear droop control for load sharing in low voltage DC distribution grid," in *Proc. IEEE Southern Power Electron*. Conf., 2017, pp. 1–6.

[19] Y. Lin and W. Xiao, "Novel Piecewise Linear Formation of Droop Strategy for DC Microgrid," in *IEEE Transactions on Smart Grid*, vol. 10, no. 6, pp. 6747-6755, Nov. 2019.

[20] Sucheng Liu, Jiazhu Zheng, Zhongpeng Li & Xiaodong Liu, "A general piecewise droop design method for DC microgrid", *International Journal of Electronics*, Vol. 108, no.5, pp.758-776, May 2021.

[21] Liu, S., Zheng, J., Li, Z., Li, R., Fang, W., & Liu, X., "Distributed Piecewise Droop Control of DC Microgrid with Improved Load Sharing and Voltage Compensation", in *2019 IEEE Third International Conference on DC Microgrids* (ICDCM) pp. 1-6, May 2019.

[22] H. Hussaini, T. Yang, Y. Gao, C. Wang, M. Urrutia and S. Bozhko,"Optimal Droop Control Design Using Artificial Intelligent Techniques for Electric Power Systems of More-Electric Aircraft," in *IEEE Transactions on Transportation Electrification*, vol. 10, no. 1, pp. 2192-2206, March 2024.

[23] M. Veysi, J. Aghaei, M. R. Soltanpour, M. Shasadeghi, B. Bahrani and D. J. Ryan, "Robust, Accurate, and Fast Decentralized Power Sharing Mechanism for Isolated DC Microgrid Using Droop-Based Sliding-Mode Control," in *IEEE Transactions on Smart Grid*, vol. 13, no. 6, pp. 4160-4173, Nov. 2022.

[24] H. Abedini and P. Mattavelli, "An Oversampled Hysteresis Modulation for Shaping the Output Impedance of Droop-Controlled Boost Converters in DC Microgrids," *2021 IEEE Fourth International Conference on DC Microgrids (ICDCM)*, Arlington, VA, USA, 2021, pp. 1-6.

[25] P. Zhao, Z. Liu and J. Liu, "An Adaptive Discrete Piecewise Droop Control in DC Microgrids," in *IEEE Transactions on Smart Grid*, vol. 15, no. 2, pp. 1271-1288, March 2024.

[26] M. Ramana, S. B. Santra, S. Prakash Gautam and A. K. Pati, "Analysis, Requirements and Boundary Condition of Droop Control in Multiple Parallel Connected Converters in DC Microgrid," *2022 4th International Conference on Energy, Power and Environment* (ICEPE), Shillong, India, 2022, pp. 1-6.

[27] Fang Chen; Wei Zhang; Burgos, R.; Boroyevich, D., "Droop voltage range design in DC micro-grids considering cable resistance," *Energy Conversion Congress and Exposition* (ECCE), 2014 IEEE, vol., no., pp.770,777, 14-18 Sept. 2014.

[28] C. M. Wildrick, F. C. Lee, B. H. Cho, and B. Choi, "A method of defining the load impedance specification for a stable distributed power system," *IEEE Trans. Power Electron*., vol. 10, no. 3, pp. 280–285, May 1995.

[29] R. D. Middlebrook, "Input filter considerations in design and application of switching regulators," in *Proc. IEEE Ind. Appl*. Soc. Annu. Meeting, 1976.

[30] Z. Huang, S. -C. Wong and C. K. Tse, "Revisiting stability criteria for DC power distribution systems based on power balance," in *CPSS Transactions on Power Electronics and Applications*, vol. 2, no. 1, pp. 76-85, 2017

[31] Y. Liao and X. Wang, "Impedance-Based Stability Analysis for Interconnected Converter Systems With Open-Loop RHP Poles," in *IEEE Transactions on Power Electronics*, vol. 35, no. 4, pp. 4388-4397, April 2020

[32] M. Wu and D. D.-C. Lu, "A novel stabilization method of LC input filter with constant power loads without load performance compromise in DC microgrids," *IEEE Trans. Ind. Electron*., vol. 62, no. 7, pp. 4552–4562, Jul. 2015.

[33] M. Su, Z. Liu, Y. Sun, H. Han, and X. Hou, "Stability analysis and stabilization methods of dc microgrid with multiple parallel-connected DC–DC converters loaded by CPLs," *IEEE Trans. Smart Grid*, vol. 9, no. 1, pp. 132–142, Jan. 2018.

[34] R. W. Erickson and D. Maksimovic, Fundamentals of Power Electronics. Berlin, Germany: Springer, 2001.

Makireddi Ramana received the B.Tech degree in electrical and electronics engineering from Andhra University, Visakhapatnam, Andhra Pradesh, India, in 2010,and M.Tech. degree in control systems engineering from the Indian Institute of Technology, Kharagpur, West Bengal, India, in 2013, and pursuing the Ph.D. degree in electrical engineering from the Jadavpur University , Kolkata, India. His main interests include Development of Control Methodologies for Power Electronic DC-DC converters in renewable energy applications.

This article has been accepted for publication in IEEE Journal of Emerging and Selected Topics in Power Electronics. This is the author's version which has not been fully edited and content may change prior to final publication. Citation information: DOI 10.1109/JESTPE.2024.3486554

Subhendu Bikash Santra (M'15, SM'22) was born in Paschim Midnapur, West Bengal, India, in 1989. He received the M.E. degree in electrical engineering with specialization in Machine and Drive and Ph.D (Engg.) with specialization in Power Electronics from Jadavpur University, Kolkata, India, in 2012 and 2023 respectively. During 2013–2014, he was an Institute Research Scholar in power electronics with the Department Electrical Engineering. IIT- Kharagpur. During 2014–2015, he was an Electrical Engineer (E&M) with Rail Vikas Nigam Limited (Schedule A PSU under Ministry of Railways, Government of India), where he designed Earth Mat for Elevated Metro Station and Lightning Protection for Station building. He also served as an Assistant Professor in electrical engineering Department at KIIT-DU, BBSR Odisha during 2015 - 2023. He is also a TARE Fellow of SERB (Govt. of India) in 2021.

He is currently an Assistant Professor with department of electrical engineering Shiv Nadar Institution of Eminence, Delhi NCR. His main research interests include DC–DC converter topologies, high-power-density converter, control of power converters, and permanent magnet synchronous motor (PMSM)/brushless dc motor motor drives. Dr. Santra is currently an Associate Editor for the International Journal of Power Electronics (Inderscience Publishers) Journal, e-Prime (Elsevier) Journal and a Member of the Institution of Engineers (India). He is also a Reviewer for the IEEE Transactions on Industrial Electronics, the IEEE Transactions on Power Electronics, the IEEE Transactions on Vehicular Technology, and the IET Power Electronics.

Debashis Chatterjee was born in Kolkata, India, in 1969. He received the Bachelor's and Ph.D. degrees from Jadavpur University, Kolkata, India, in 1990, and 2005, respectively, and the M.Tech. degree from IIT Kharagpur, Kharagpur, India, in 1992, all in electrical engineering. From 1992 to 2002, he was a Sr. Design Engineer with NELCO, New Delhi, and Crompton Greaves Ltd., Mumbai, India, where he worked on industrial drives and automation division, and an Assistant Manager for lighting electronics design with Philips India Ltd., New Delhi, India. He is currently a Professor with the Department of Electrical Engineering, Jadavpur University. His research interests include electrical machines, variable-speed drives, electric vehicles, renewable energy generation, and power quality study.

Yam Siwakoti received the B.Tech. degree in electrical engineering from the National Institute of Technology, Hamirpur, India (2005), the master's degree in electrical power engineering from the Norwegian University of Science and Technology, Trondheim, Norway, and Kathmandu University, Dhulikhel, Nepal (2010), and the Ph.D. degree in electronic engineering from Macquarie University, Sydney, Australia (2014). He was a Postdoctoral Fellow with the Department of Energy Technology, Aalborg University, Denmark (2014-2016). He was a Visiting Professor at the Department of Engineering Science, University of Oxford, Oxford, UK (2023). He was also a Visiting Scientist with the Fraunhofer Institute for Solar Energy Systems, Freiburg, Germany (2018 & 2023). His research has been recognized by a series of awards and recognition including the most prestigious Friedrich Wilhelm Bessel Research Award from the Alexander von Humboldt Foundation, Germany (2022), and the Green Talent Award from the Federal Ministry of Education and Research, Germany (2016). He was also recognized as a "Field Leader" in Power Engineering by The Australian's annual Research Magazine (2023). Dr. Siwakoti is currently an Associate Professor at the University of Technology Sydney. He is also serving an Associate Editor of IEEE Transactions on Power Electronics, IEEE Transactions on Industrial Electronics and IEEE Journal of Emerging and Selected Topics in Power Electronics.